HHS Public Access

Author manuscript

Nat Struct Mol Biol. Author manuscript; available in PMC 2010 December 23.

Published in final edited form as:

Nat Struct Mol Biol. 2009 December ; 16(12): 1252–1258. doi:10.1038/nsmb.1717.

Physical determinants of strong voltage sensitivity of K^+ channel block

Yanping Xu[*], **Hyeon-Gyu Shin**[*], **Szilvia Szép**, and **Zhe Lu**

Department of Physiology, Howard Hughes Medical Institute, University of Pennsylvania, 3700 Hamilton Walk, Philadelphia, PA 19104

Abstract

Strong voltage sensitivity of inward-rectifier K^+ (Kir) channels has been hypothesized to arise primarily from an intracellular blocker displacing up to five K^+ ions from the wide, intracellular part of the ion conduction pore outwardly across the narrow ion selectivity filter. The validity of this hypothesis depends on two assumptions: i) that five ion sites are located intracellular to the filter, and ii) that the blocker can force essentially unidirectional K^+ movement in a pore region generally wider than the combined dimensions of the blocker plus a K^+ ion. Here, we present a crystal structure of the cytoplasmic portion of a Kir channel with five ions bound, and demonstrate that a constriction near the intracellular end of the pore, acting as a gasket, prevents K^+ ions from bypassing the blocker. This heretofore unrecognized "gasket" ensures that the blocker can effectively displace K^+ ions across the selectivity filter to generate exceedingly strong voltage sensitivity.

Many pharmacological agents, as well as endogenous biological molecules, act by blocking ion channels in a voltage-dependent manner[1]. The earliest and most dramatic example of such action is the "anomalous" voltage dependence of inwardly rectifying K^+ (Kir) conductance discovered by Sir Bernard Katz six decades ago[2]. He observed that, contrary to the classic voltage-gated K^+ (Kv) conductance, the Kir conductance tends to zero with membrane depolarization and increases with hyperpolarization, a diode-like behavior originally termed anomalous rectification[2] and later inward rectification[3]. The voltage sensitivity of Kir channels arises from voltage-dependent block of their ion pore by intracellular cations such as the polyamine spermine[4–6]. For the past three decades, voltage dependence of ion channel block has generally been assumed, by analogy with proton block of voltage-gated Na^+ channels[7], to reflect the transit of the charged blocker across the transmembrane electric field. Departing from this prevalent view, our group posits that the high valence of 4 – 5 associated with block of strong rectifiers primarily reflects the movement, not of tetravalent spermine itself, but of up to five K^+ ions "displaced" by

Please send correspondence to: Dr. Zhe Lu, University of Pennsylvania, Department of Physiology, A202 Richards Building, 3700 Hamilton Walk, Philadelphia, PA 19104, Tel: 215-573-7711, FAX: 215-573-1940, zhelu@mail.med.upenn.edu.

[*]These authors contributed equally.

AUTHOR CONTRIBUTIONS

Y. X., H. S. and Z.L. performed the experiments; Y.X., H.S., S.S. and Z.L. analyzed the data; Y.X. and Z.L. wrote the manuscript; Y.X. and H.S. contributed equally to this work.

spermine across the steep electric field in the narrow K^+ selectivity filter[8,9] (Fig. 1a). This latter type of mechanism was originally proposed to underlie the modest voltage dependence of Kv channel block by tetraethylammonium (TEA; valence < 1)[10] (see also Ref. 11).

Structures of two full-length Kir channels have been determined: bacterial KirBac1.1 and a Kir chimera formed by joining the transmembrane portion of a bacterial Kir to the cytoplasmic portion of eukaryotic Kir3.1[12,13]. The transmembrane portion of a Kir pore resembles that of KcsA: its outer, narrow, and K^+-selective part is formed by the signature sequence whereas the remaining part is lined by the second transmembrane (M2) segment (Fig. 1b; PDB 2QKS[13]). This transmembrane pore is extended into the cytoplasm by the so-called cytoplasmic pore[14,15] formed mostly by the C-terminus. We will refer to the combination of M2 and the cytoplasmic portions of the pore as the inner pore which, unlike the selectivity filter, does not highly discriminate among alkali metal ions. Using Rb^+ as K^+ surrogate, three ion sites, in addition to the four sites (S1 – S4) in the selectivity filter, were identified in the inner pore of the chimeric Kir[13]. One of these (denoted S5) is located in the so-called cavity, a wider pore region just internal to the selectivity filter and lined by the second transmembrane (M2) segment (Fig. 1b). The other two (S6 and S7) are located on either side of the G-loop at the external end of the cytoplasmic pore. The electron density peaks at these latter sites are too low to represent full ion occupancy, and it is therefore unclear whether they are alternative sites. Here, using eukaryotic Kir channels, we set out to investigate certain key requirements for using the blocker-K^+ displacement model to account for inward rectification.

RESULTS

Five ion sites within the cytoplasmic pore

The blocker-K^+ displacement model predicts the presence of many ions in the large and seemingly “empty” cytoplasmic pore (Fig. 1b). To obtain structural evidence for such occupancy, we crystallized the isolated cytoplasmic pore of the Kir3.1 channel with the S225E mutation (see below). After screening a very large number of conditions, we obtained an interesting crystal of the (mutant) cytoplasmic pore protein grown in a solution with Na^+ as K^+ surrogate, and solved its structure at 2.0 Å resolution (see Online Methods) by means of molecular replacement using a wild-type structure (PDB 1N9P[14]). Fig. 2a shows part of the crystal structure model of the cytoplasmic pore (with ions and relevant water molecules), superimposed on a $2F_o – F_c$ composite-omit electron density map (see Supplementary Fig. 1 for the entire structure). It was calculated using a model lacking all water molecules and ions, as well as any side chains (shown as sticks) that interact directly or through water molecules with the newly identified ions. This electron density map, contoured at 2.5 σ, exhibits five density peaks along the central axis of the cytoplasmic pore. The most external one corresponds to S7 in the chimeric Kir[13], whereas the four internal ones (S8 – S11) are newly observed (Figs. 2a, b). Including S8 – S11, the pore of a Kir channel may therefore contain as many as eleven ion sites (Fig. 2b).

The S10 ion is uniquely located within a bracket formed by four symmetric Phe255 benzyl side chains, implicitly stabilized by π – cation interactions (Fig 2a, c). Phe255 is located within the cytoplasmic loop, and the four symmetric loops constrict an intracellular part of

the pore to < 10 Å (Fig. 2a, b). At all other ion sites, mostly oxygen-containing side chains extend, through water molecules, negative dipole moments towards Na^+. The water molecules around the S7 ion are anchored to the Thr309 side-chain (and possibly G307 carbonyl) oxygen(s) (Fig. 3a). The mutant Glu225 side chain appears to interact with the S8 ion both electrostatically and via water molecules (Fig. 3b). We introduced this S225E mutation because functional studies suggest K^+ interacts with the corresponding Glu224 of Kir2.1[16–18]. The S9 ion interacts with two sets of four water molecules, located on planes internal (dark green spheres) and external (light green spheres) to the ion (Fig. 3c). The external set is anchored to Gln227 and Gln261 whereas the internal one is indirectly anchored to Asp260 via another water molecule. The S11 ion is located in the cytoplasmic vestibule that contains a large number of water molecules (Fig. 3d). The distance between Na^+ ions and their surrounding water molecules (Supplementary Table 1) is generally greater than the optimal distance for Na^+-O interactions[19]. In the cytoplasmic pore, the water molecules interact with Na^+ located on the central axis and side-chain oxygens on the perimeter. Such spatial constraints could prevent water molecules from attaining optimal distances (on average), resulting in weak interactions. While weak interactions would allow ions to traverse the cytoplasmic pore at the expected near diffusion-limited rates, longer interaction distances would also comfortably accommodate the larger K^+ ions.

Spermine produces strong voltage sensitivity by displacing K^+ ions

Fig. 4a shows macroscopic currents of wild-type and four mutant Kir2.1 channels, recorded in the absence or presence of the intracellular polyamine spermine. Previous studies have shown that spermine blocks Kir2.1 in (at least) two sequential steps[9,20,21]. Consequently, the (voltage-dependent) blocking curve exhibits a shallow and a steep phase (filled circles, Fig. 4b), reflecting spermine binding at the shallow and the deep site, respectively. Our group[21] has shown that substituting alanine for Kir2.1's Phe254 (corresponding to Kir3.1's Phe255; Fig. 2a) eliminates the shallow phase of the blocking curve (filled diamonds, Fig. 4b). This finding suggests that the aromatic side chain contributes to the shallow site, and predicts that only mutant channels with aromatic substitutions at Phe254 will have wild-type characteristics. Indeed, F254W and F254Y mutant channels each exhibit both a shallow and a steep voltage-dependent blocking phase, and the shapes of their blocking curves (Fig. 4b) are nearly indistinguishable from that of wild-type channels. In contrast, F254V channels exhibit a single steep phase (Fig. 4b) closely resembling that of F254A mutants. The voltage dependence of spermine binding at this F254 site has an effective valence of 0.4, as quantified from the slope of the shallow blocking phase[9]. Given the (near) absence of a trans-cytoplasmic pore electric field, it must reflect outward displacement by spermine of the K^+ ion present at the site.

Leaving the shallow site, spermine proceeds to a deeper (Fig. 5a) and much higher-affinity site, with ten-fold stronger voltage dependence (valence = 4.2)[9, 21]. If spermine in the deep blocked state is predominantly positioned internal to the narrow selectivity filter, and if it generates voltage dependence primarily by displacing K^+ ions across the selectivity filter, then certain inner pore mutations should eliminate the high-affinity and strongly voltage-dependent spermine block. It has long been known that a neutral mutation of Asp172 in the cavity (Fig. 5a) affects rectification[8, 16, 22–24]. However, considering that this mutation

lowers the deep-site affinity for spermine by < 3 kcal/mol at 0 mV[8,18], ~1/3 of the total binding energy, a long spermine molecule in the deep blocked state must have additional significant interactions with the pore. We therefore systematically substituted alanine for each residue (valine for native alanine) in the pore-lining stretch of M2 (from C169 to K188). Fifteen of the 20 mutants express sufficient current for patch recording. While these M2 mutations, as expected, have little influence on spermine affinity at the shallow site (Fig. 5b), four of them (D172A, F174A, I176A and M183A) significantly lower the affinity of the deep site (Fig. 5c). Put in perspective, the estimated perturbation energy (ΔΔG) due to these four mutations is ~7 kcal/mol, compared with the ~8 kcal/mol free energy ($K_d \approx 2$ μM)[9] estimated for spermine binding in the deep blocked state. Since the individual mutations separately perturb the interaction of spermine with Kir2.1 only modestly, the deep spermine-binding locus should remain relatively well defined in each of those mutant channels. Intriguingly, the four effective mutations in M2 are spread over three α-helical turns, about the distance (~17 Å) between the two end nitrogen atoms of spermine. Each of the four relevant residues may or may not directly interact with spermine. Nevertheless, given that mutations outside this three-turn region do not significantly affect spermine block, it is reasonable to conclude that the four residues approximately delineate the predominant, most strongly voltage-dependent binding locus of spermine in M2.

To reduce maximally the affinity of the inner pore for spermine, we combined various mutations in both M2 (D172, F174, I176 and M183) and the cytoplasmic pore (E224, F254, D255 and E299) that are known to affect spermine block (Figs.4 and 5) (Refs. 15–18, 21–25). We obtained a quintuple-alanine mutant (termed 5A, featuring D172A, I176A, and M183A in M2, and E299A and F254A in the cytoplasmic pore, all corresponding residues colored yellow in Fig. 6a) that expresses sufficient current for patch recording. Whereas 1 μM spermine causes profound voltage-dependent block of wild-type current, even 1 mM spermine has little effect on the 5A mutant (Fig. 6b–f). Given that simultaneous mutation of five residues, all located internal to the selectivity filter (Fig. 6a), abolishes specific spermine binding to the channel (Fig. 6d–f), the selectivity filter itself evidently must have little inherent affinity for spermine.

Four symmetric loops near the internal end of the pore act as a gasket

To generate a valence of 4 – 5, spermine must not only penetrate sufficiently deep into the inner pore to displace four to five K^+ ions but also displace them almost exclusively outwardly. The following information, however, strongly implies that, without special structural constraints, such obligatory displacement is unlikely to occur. The inner pore is wide and ions within it are unlikely to stay in true single file. Indeed, the Ussing flux-ratio exponent of Kir2.1 is only 2.2 (Ref. 26), which suggests that K^+ ions mix (i.e., exchange positions) inside the inner pore. This inference in turn raises the question: why do K^+ ions all (or nearly all) move outwardly through the ion selectivity filter instead of bypassing the blocker and leaking into the intracellular solution as, apparently, occurs in Kv channels? For example, although intracellular TEA blocks Kv channels by displacing the K^+ ion[10] from its binding site in the cavity, the observed valence of TEA block is only ~0.2 rather than about one[27–31]. Such low valence strongly implies that the K^+ ion in the cavity of a Kv channel has a high probability of leaking back into the intracellular solution, not obligatorily moving

outwardly across the selectivity filter to generate voltage dependence. What structural constraint prevents such leak in Kir channels? To address this question, we focused on the four symmetric cytoplasmic loops that constrict the pore near its intracellular end to < 10 Å (Figs. 2a, 6a), asking whether these loops function as a "gasket" that encircles the blocker and prevents K^+ ions from leaking into the intracellular solution. We deleted four (GFDS) of the five (GFDSG) residues that form the cytoplasmic loop (boxed region, Fig. 6a), leaving a single glycine to join the two ends. The expectation was that, if the loops indeed function as a gasket, their removal will lower the apparent voltage dependence of channel block. If the outward and inward escape probabilities become equal, the valence should drop by 50%. For reasons explained below, we used a spermine derivative, phenyl-propyl-spermine (PP-spermine; Fig. 7a), instead of spermine itself to carry out this particular study. PP-spermine (1 μM) inhibits the Kir2.1 current in a voltage-dependent manner. The blocking curve exhibits only the deep, not the shallow, phase because the blocker concentration we used is too low to significantly populate the shallow blocked state [K_d(0 mV) for spermine is > 0.1 mM[9]; Fig. 4]. A single Boltzmann curve makes it easier to visualize the mutation-induced reduction of the apparent valence of channel block from the shallowing of the slope of the blocking curve. Channels without the loops display a discernibly shallower blocking curve (valence 2.5, down 42% from 4.3) but little change in overall affinity for spermine (Fig. 7b–d). The two-unit drop in valence suggests that, in the absence of the cytoplasmic loops, two K^+ ions on average leak back into the intracellular solution.

Four factors could potentially confound our interpretation of the deletion mutant's behavior discussed above. First, spermine pops through the selectivity filter with a low probability (0.02) and at a low rate (10 s^{-1})[9],[32]. This property causes a small hump in the voltage-dependent blocking curve, more prominent at low (e.g., 1 μM) spermine concentration (Fig. 6f). In principle, a mutation-induced increase in spermine pop-through rate could decrease the apparent voltage dependence. To avoid this potential problem, we used PP-spermine (Fig. 7a) whose bulky head group precludes such undesirable pop-through (Fig. 7b). As already mentioned, at 1 μM, PP-spermine occupancy at the shallow blocker site should be minimal because of that site's very low affinity for amine blockers. Indeed, Kir2.1 block by 1 μM PP-spermine is well described by a single Boltzmann function (Fig. 7b), and its voltage dependence is so strong (valence > 4, Fig. 7d) that it must reflect binding at the deep site. This latter inference is further supported by the finding that the F254A mutation in the cytoplasmic loop, which is known to abolish the shallow site[21] (Fig. 4), barely affects the blocking curve (Fig. 7e). A suitable substitute for spermine, PP-spermine (Fig. 7d) blocks wild-type channels with practically the same voltage dependence (Z = 4.3) as spermine itself (Z = 4.6)[9]. Second factor: given that F254 within the deleted loop is essential for the shallow blocker site, the observed drop in valence might be indirectly caused by the loss of the shallow site. This is however not the case because the pure F254A mutation (which eliminates the shallow site[21]) itself barely lowers the steepness of the blocking curve (Fig. 7d, e). Third, deleting the loop near the internal entrance to the pore could, in principle, prevent PP-spermine from accessing the deep blocker site and thereby reduce the voltage dependence. To the contrary, PP-spermine actually blocks the loop-deleted mutant channel with a K_d practically identical to that of the deep site of wild-type channels (Fig. 7c). Finally, to rule out the fourth possibility that the reduced valence is an epiphenomenon

peculiar to PP-spermine block, we show that a similar phenomenon also occurs with decane-bis-trimethylammonium (bis-QA_{C10}), a compound of very different structure and chemistry (Fig. 7a, f, g). Having ruled out these potentially confounding factors, we conclude that the four cytoplasmic loops effectively function as a gasket, preventing K^+ ions from leaking inwardly and thereby ensuring their effective outward displacement.

DISCUSSION

We report here several important novel findings. First, the cytoplasmic pore itself contains five ion sites (Fig. 2a, b), which brings the number of identified ion sites in the pore of a Kir channel to as many as eleven. Second, spermine produces the observed maximal voltage sensitivity as its leading end penetrates into the cavity (Fig. 5). Five mutations, all internal to the selectivity filter, essentially abolish spermine block (Fig. 6). These results do not support the view that tetravalent spermine produces voltage sensitivity by penetrating deep into the narrow selectivity filter, but rather the view that the voltage sensitivity primarily results from the movement of displaced K^+ ions[8,9] (compare Refs. 33, 34). If the voltage dependence of block does not reflect spermine entry into the selectivity filter, a blocker with head groups too wide to enter the filter should block channels with similar voltage dependence. Indeed, bis-QA_{C10} (Fig. 7a), comparable in length to spermine but with two fewer charges, blocks channels with practically the same voltage dependence[9] (Fig. 7d, g), even though the trimethyl head group (~6 Å) of bis-QA_{C10} is about twice as wide as the selectivity filter. Our third finding is that deletion of the cytoplasmic loops, which constrict the pore to ~10 Å (Figs. 2a, 6a), lowers the apparent valence of polyamine block by about half (Fig. 7b, d). The constriction created by the cytoplasmic loops effectively functions as a gasket, preventing K^+ ions from bypassing the blocker and leaking into the intracellular solution, and thereby enabling an advancing blocker to force K^+ ions to move nearly exclusively across the selectivity filter.

As a spermine molecule enters the Kir2.1 pore, it first binds at a shallow site (S10, Fig 2) formed by four symmetric phenyl rings, in a weakly voltage-sensitive step. The apparent valence (0.4) of this step[9] suggests that functional K^+ occupancy of the site is at least 0.4. If in reality S10 is fully occupied by K^+, the ion's chances of being displaced in the outward direction or escaping into the intracellular solution must have been comparable. As for the S11 ion, given its location in the very wide vestibule (Fig. 2), it can easily bypass spermine and escape into the intracellular solution and not be forced to move in the outward direction. In moving from the shallow site (likely via additional intermediate sites) to the cavity region, spermine generates strong voltage sensitivity (valence ~4)[9] primarily by displacing K^+ ions at S5 – S9. It follows that, in the functional study, averaged K^+ occupancy at these five sites is ~0.8, that is, only four of the five ion sites are occupied at any time. The constriction on the cytoplasmic side formed by four symmetric loops, acting as a "gasket", ensures that spermine effectively displaces (nearly) all the ions toward the extracellular solution.

Regarding ion sites within the cytoplasmic pore, two structural features deserve further discussion. First, the S10 ion in the isolated cytoplasmic pore structure is apparently suspended in the π electron field of the benzyl rings (Fig. 2), a concept first introduced in K^+

channel studies to explain why aromatic side chains in a Kv channel confer millimolar affinity for extracellular TEA[35–38]. Comparison of the isolated cytoplasmic pore structure (reported here) with those of the Kir chimera previously crystallized in two different states (A and B)[13] yields clues as to how ions move in the pore. In the former, the benzyl side chains of four Phe255 (colored yellow) form a cage where an ion is suspended by the π electron field (Figs. 2 and 8a). The distance between the S10 ion and the centroid of each phenyl ring is 5.5 Å, within the preferred range for a π – cation interaction[39]. In contrast, the benzyl side chains in the two chimeric structures adopt different χ_1 and/or χ_2 angles ($\Delta\chi_1$ = 50° and $\Delta\chi_2$ = 20° in state A; $\Delta\chi_1$ = −20° in B), pointing in either the intracellular (state A, blue) or the extracellular (state B, gray) direction (Fig. 8a). Consequently, in either chimeric structure, the side chains are too far apart to hold an ion. The cage-like arrangement of four Phe255 side chains in the isolated cytoplasmic pore may therefore result from π - cation interactions rather than reflect inherent natural tendencies of the side chains themselves. It seems that as an ion from the intracellular vestibule enters the pore, moving from S11 to S10, the benzyl rings swing toward S10 from their chimera state A position to that in the cytoplasmic pore structure, capturing the ion (Fig. 8a). In similar fashion, the benzyl rings may swing from their chimera state B position toward S10, capturing an ion coming from S9. Notably, the electron density at S10 is somewhat elongated axially (Fig. 2a), which implies some oscillation of the ion at that site. Once it, or the benzyl side chains, move too far to interact with one another, the ion is free to proceed to an adjacent site and the phenyl rings may then move apart to assume the positions seen in the chimeric structures. Thus, the three structures compared here may represent individual snapshots of ion motion along the intracellular end of the pore. Given that χ-angle motion of (structurally unrestrained) phenylalanine side-chains occurs on a sub-nanosecond time scale[40], residence of an ion at S10 is expected to be so brief that transit rate across the site will be near diffusion limited.

Another difference in the conformation of side-chain rotamers between the isolated cytoplasmic pore and its chimeric counterpart[13] appears to affect ion residence at S9. In the former, the side chain of Arg229 is hydrogen bonded to Glu300 (upper panel, Fig. 8b), whereas in the Kir chimera (state B), it extends into the pore (lower panel). (In state A the side chain alternates between the two rotamer conformations.) Pointing the side chain of Arg229 into the pore may affect ion binding at S9 in two ways (Fig. 8b). First and intuitively, the positively charged side chain increases the electrostatic potential near S9 (lower panel) and conversely, the S9 ion repels the side chain of Arg229 from the pore (upper panel). Second, a side-chain nitrogen (η^1) of Arg229 becomes hydrogen bonded to the side-chain oxygen (ε^1) of Gln227 (lower panel), not that of Glu300 (upper panel) as in the isolated cytoplasmic pore structure. The side-chain nitrogen (ε^2) of Gln227 (in the chimera structure) is in turn hydrogen bonded to the side-chain oxygen (ε^1) of Gln261. Consequently, ε^1 oxygens of both Gln227 and Gln261 are no longer available to anchor the water molecule coordinating the S9 ion (Fig. 8b). These arrangements help explain the absence of an ion at S9 in the chimera structure.

In the cytoplasmic pore, the ion-binding sites are formed mainly by certain side chains in specific rotamer conformations. Thus, thermal energy-driven side-chain motion will cause ion sites to appear and disappear on a sub-nanosecond time scale, enabling ions to move across their sites at near diffusion-limited rates, while the direction of net K^+ movement is

determined by the electrochemical potential. Ions interact either with aromatic side chains or with water molecules anchored to protein oxygens (Figs. 2 and 3). Given this anchoring, the water molecules' dipole moment must be oriented in such a way that it can only interact with a cation not an anion, a feature that helps prevent anion accumulation in the pore. The presence of this large number of K^+ ions in the cytoplasmic pore sets the stage for spermine to produce strongly voltage-dependent block. Spermine penetrates deep into the inner pore, displacing the ions from the inner pore across the selectivity filter to produce strong voltage sensitivity (Fig.1a), even though tetravalent spermine itself does not enter the filter and therefore does not directly sense the steep electric field that drops across it. In fact, over four decades ago, Hodgkin and Horowitz[41] found that Kir conductance varies with the difference between membrane voltage (V_m) and the K^+ equilibrium potential (E_K), and concluded that: "the potassium permeability [now ascribed to Kir channels] varies greatly with the force acting on the potassium ions". Subsequently, Hagiwara and Takahashi[42] demonstrated that the relative conductance (G/G_{max}) is quantitatively described by the empirical equation

$$\frac{G}{G_{\max}}(\Delta V)=\frac{1}{1+e^{\left(\frac{\Delta V-\Delta V_{1/2}}{\nu}\right)}}. \quad \text{Eq.1}$$

That is, G/G_{max} (at constant $[K^+]_{int}$[43,44]) is a function of ΔV, the difference between V_m and E_K, not of V_m per se ($\Delta V_{1/2}$ is the ΔV at which G/G_{max} becomes 0.5, and ν is a steepness factor).

In the framework of the simple blocker-K^+ displacement model of Fig. 1a, the expression derived for relative conductance[8,45],

$$\frac{G}{G_{\max}}=\frac{1}{1+\frac{[B]}{\left[K^+_{\text{int}}\right]^n K_{eq}(0mV)e^{-\frac{nZ_K F(V_m-E_K)}{RT}}}}, \quad \text{Eq.2}$$

corresponds exactly to the empirical equation of Hagiwara and Takahashi[42]. ([B] and $[K^+_{int}]$ are blocker and intracellular K^+ concentrations, K_{eq} is the apparent equilibrium constant of blocker binding, Z_K is the valence of K^+, n is the number of K^+ ions displaced, and F, R and T have their usual meaning). Comparison of equation 1 and equation 2 reveals the theoretical underpinnings of the empirical parameters in Hagiwara and Takahashi's equation:

$$\Delta V_{1/2}=\frac{RT}{nZ_K F}\ln\frac{[K^+_{\text{int}}]^n K_{eq}(0mV)}{[B]}, \text{ and } \nu=\frac{RT}{nZ_K F}.$$

In summary, the following principles effectively confer strong voltage dependence on K^+ channel block. First, an intracellular cationic blocker and extracellular permeant (K^+) ions (electrostatically) displace one another and/or bind competitively to the inner pore from opposite sides[8–11]. This process energetically couples blocker binding to the movement of K^+ ions. Second, as the blocker traverses the relatively wide inner pore, K^+ ions move across the narrow selectivity filter; the movement of K^+ ions, not of the blocker, is primarily voltage dependent. Third, the number of K^+ ions that reside in the inner pore sets an upper

bound to the steepness of the voltage dependence. Fourth, a narrowing near the intracellular end of the pore functions as a gasket to prevent K^+ ions from bypassing the blocker and leaking into the intracellular solution. This latter, heretofore unrecognized, structural constraint underlies the nearly obligatory coupling between intracellular blocker binding and outward K^+ ion movement in Kir channels, by which the blocker-binding reaction acquires its characteristic strong voltage sensitivity.

METHODS

Molecular Biology

The cDNA of Kir2.1[46] was in pGEM-Hess plasmid[47], and the joined cDNA fragments encoding the N- and C-termini of Kir3.1[48],[49] was in pET28b(+) vector[14]. We made all cDNA mutations using a PCR-based method, and synthesized cRNAs with T7 polymerase (Promega Corp., Madison, WI) using linearized cDNA as a template.

Electrophysiological recordings

We recorded macroscopic currents from inside-out membrane patches of *Xenopus* oocytes (previously injected with corresponding cRNAs) using an Axopatch 200B amplifier (MDS Analytical Technologies), filtered at 10 kHz and sampled at 100 kHz using a Digidata 1322A analog-to-digital converter (MDS Analytical Technologies) interfaced with a personal computer. We used pClamp8 software (MDS Analytical Technologies) to control the amplifier and data acquisition. We subtracted the background current from the total current as previously described[50]. The recording solution contained (mM): 5 K_2EDTA, 10 "K_2HPO_4 + KH_2PO_4" in a ratio yielding pH 8.0, and sufficient KCl to bring total K^+ concentration to 100 mM[51]. To minimize channel rundown the intracellular solution contained 5 mM fluoride, 10 mM pyrophosphate and 0.1 mM vanadate[52].

Protein production, crystallography and structure determination

We produced the intracellular domain protein of Kir3.1 containing the S225E mutation with an *E. coli* expression system as previously described[14]. This domain, joining the N-terminal residues 41 – 63 and C-terminal residues 190 – 371, contains a N-terminal His-tag followed by a thrombin-cutting site. We grew the protein crystal at 4°C by vapor diffusion in sitting drops. We mixed the protein at 8–12 mg/ml with an equal volume of reservoir solution [100 mM tri-sodium citrate, 200 mM ammonium acetate, 5 mM Ba^{2+}, 28% 2-methyl-2,4-pentanediol (MPD); pH 5.5]. We flash froze the crystal in liquid nitrogen and kept it at 95 K during diffraction. We collected the diffraction data at a synchrotron source (National Synchrotron Light Source, beam line X25) tuned to a wavelength of 1.1 Å. We carried out indexing, integration, and scaling of the data with DENZO and SCALEPACK, and further processing with the CCP4 package[53],[54]. We performed molecular replacement with AMoRe[55] using a wild-type structure as model (PDB 1N9P)[14], and refined the molecular replacement model against the data alternatingly in real and reciprocal space using programs O or Coot, and CNS[56]–[58], respectively. We validated the final model with PROCHECK[59]: 91.9%, 8.1%, and 0% residues are in favored, allowed, and outlier regions, respectively. We prepared structure figures with PyMOL[60], Origin 8.0 (OriginLab Corp.) and CorelDraw10 (Corel Corp.).

Accession code

Protein Data Bank: The atomic coordinates and structure factors for the S225E-mutant Kir3.1 cytoplasmic pore have been deposited in Protein Data Bank with accession code 3K6N.

Supplementary Material

Refer to Web version on PubMed Central for supplementary material.

ACKNOWLEDGMENT

We thank L. Jan (University of California, San Francisco) for sharing Kir2.1 and Kir3.1 cDNAs, J. Yang (Columbia University) for Kir2.1 cDNA in the pGEM-Hess vector; R. MacKinnon (Rockefeller University) for Kir3.1 cytoplasmic-pore cDNA construct and for teaching molecular replacement method to Z. Lu; R. Dominguez, K. Ferguson, S. Lee, S. Li, K. Schmitz, and Y. Zhou for technical assistance and/or discussion, staff at CHESS A1 and NSLS X25 for technical service; and P. De Weer for review and discussion of our manuscript. This study was supported by a grant (GM55560) from the National Institutes of Health. Zhe Lu is an investigator of the Howard Hughes Medical Institute.

REFERENCES

1. Hille, B. Ion Channels of Excitable Membranes. 3rd edition.. Sunderland, MA: Sinauer Associates; 2001.
2. Katz B. Les constantes électriques de la membrane du muscle. Archives des Sciences Physiologiques. 1949; 3:285–299.
3. Noble D. Electrical properties of cardiac muscle attributable to inward going (anomalous) rectification. J Cell Comp Physiol. 1965; 66:127–136.
4. Lopatin AN, Makhina EN, Nichols CG. Potassium channel block by cytoplasmic polyamines as the mechanism of intrinsic rectification. Nature. 1994; 372:366–369. [PubMed: 7969496]
5. Ficker E, Taglialatela M, Wible BA, Henley CM, Brown AM. Spermine and spermidine as gating molecules for inward rectifier K^+ channels. Science. 1994; 266:1068–1072. [PubMed: 7973666]
6. Fakler B, et al. Strong voltage-dependent inward rectification of inward rectifier K^+ channels is caused by intracellular spermine. Cell. 1995; 80:149–154. [PubMed: 7813010]
7. Woodhull AM. Ionic blockage of sodium channels in nerve. J. Gen. Physiol. 1973; 61:687–708. [PubMed: 4541078]
8. Guo D, Ramu Y, Klem AM, Lu Z. Mechanism of rectification in inward-rectifier K^+ channels. J. Gen. Physiol. 2003; 121:261–275. [PubMed: 12642596]
9. Shin HG, Lu Z. Mechanism of the voltage sensitivity of IRK1 inward-rectifier K^+ channel block by the polyamine spermine. J.Gen. Physiol. 2005; 125:413–426. [PubMed: 15795311]
10. Armstrong CM. Interaction of tetraethylammonium ion derivatives with the potassium channels of giant axons. J. Gen. Physiol. 1971; 58:413–437. [PubMed: 5112659]
11. Spassova M, Lu Z. Coupled ion movement underlies rectification in an inward-rectifier K^+ channel. J. Gen. Physiol. 1998; 112:211–221. [PubMed: 9689028]
12. Kuo A, et al. Crystal structure of the potassium channel KirBac1.1 in the closed state. Science. 2003; 300:1922–1926. [PubMed: 12738871]
13. Nishida M, Cadene M, Chait BT, MacKinnon R. Crystal structure of a Kir3.1-prokaryotic Kir channel chimera. EMBO J. 2007; 26:4005–4015. [PubMed: 17703190]
14. Nishida M, MacKinnon R. Structural basis of inward rectification: cytoplasmic pore of the G protein-gated inward rectifier GIRK1 at 1.8 Å resolution. Cell. 2002; 111:957–965. [PubMed: 12507423]
15. Pegan S, et al. Cytoplasmic domain structures of Kir2.1 and Kir3.1 show sites for modulating gating and rectification. Nat. Neurosci. 2005; 8:279–287. [PubMed: 15723059]

16. Yang J, Jan YN, Jan LY. Control of rectification and permeation by residues in two distinct domains in an inward rectifier K^+ channel. Neuron. 1995; 14:1047–1054. [PubMed: 7748552]
17. Taglialatela M, Ficker E, Wible BA, Brown AM. C-terminus determinants for Mg^{2+} and polyamine block of the inward rectifier K^+ channel IRK1. EMBO J. 1995; 14:5532–5541. [PubMed: 8521810]
18. Guo D, Lu Z. Interaction mechanisms between polyamines and IRK1 inward rectifier K^+ channels. J. Gen. Physiol. 2003; 122:485–500. [PubMed: 14581581]
19. Harding MM. Small revisions to predicted distances around metal sites in proteins. Acta Crystallogr. D Biol. Crystallogr. 2006; 62:678–682. [PubMed: 16699196]
20. Lopatin AN, Makhina EN, Nichols CG. The mechanism of inward rectification of potassium channels: "long-pore plugging" by cytoplasmic polyamines. J. Gen. Physiol. 1995; 106:923–955. [PubMed: 8648298]
21. Shin HG, Xu Y, Lu Z. Evidence for sequential ion-binding loci along the inner pore of the IRK1 inward-rectifier K^+ channel. J. Gen. Physiol. 2005; 126:123–135. [PubMed: 16043774]
22. Stanfield PR, et al. A single aspartate residue is involved in both intrinsic gating and blockage by Mg^{2+} of the inward rectifier, IRK1. J. Physiol. 1994; 478:1–6. [PubMed: 7965824]
23. Lu Z, MacKinnon R. Electrostatic tuning of Mg^{2+} affinity in an inward-rectifier K^+ channel. Nature. 1994; 371:243–246. [PubMed: 7915826]
24. Wible BA, Taglialatela M, Ficker E, Brown AM. Gating of inwardly rectifying K^+ channels localized to a single negatively charged residue. Nature. 1994; 371:246–249. [PubMed: 8078584]
25. Kubo Y, Murata Y. Control of rectification and permeation by two distinct sites after the second transmembrane region in Kir2.1 K^+ channel. J. Physiol. 2001; 531:645–660. [PubMed: 11251047]
26. Stampe P, Arreola J, Perez-Cornejo P, Begenisich T. Nonindependent K^+ movement through the pore in IRK1 potassium channels. J. Gen. Physiol. 1998; 112:475–484. [PubMed: 9758865]
27. French RJ, Shoukimas JJ. Blockage of squid axon potassium conductance by internal tetra-N-alkylammonium ions of various sizes. Biophys. J. 1981; 34:271–291. [PubMed: 7236852]
28. Yellen G, Jurman ME, Abramson T, MacKinnon R. Mutations affecting internal TEA blockade identify the probable pore-forming region of a K^+ channel. Science. 1991; 251:939–942. [PubMed: 2000494]
29. Choi KL, Mossman C, Aube J, Yellen G. The internal quaternary ammonium receptor site of Shaker potassium channels. Neuron. 1993; 10:533–541. [PubMed: 8461140]
30. Holmgren M, Smith PL, Yellen G. Trapping of organic blockers by closing of voltage-dependent K^+ channels: evidence for a trap door mechanism of activation gating. J. Gen. Physiol. 1997; 109:527–535. [PubMed: 9154902]
31. Zhou M, Morais-Cabral JH, Mann S, MacKinnon R. Potassium channel receptor site for the inactivation gate and quaternary amine inhibitors. Nature. 2001; 411:657–661. [PubMed: 11395760]
32. Guo D, Lu Z. Mechanism of IRK1 channel block by intracellular polyamines. J. Gen. Physiol. 2000; 115:799–814. [PubMed: 10828252]
33. Kurata HT, et al. Molecular basis of inward rectification: polyamine interaction sites located by combined channel and ligand mutagenesis. J. Gen. Physiol. 2004; 124:541–554. [PubMed: 15477380]
34. Kurata HT, Marton LJ, Nichols CG. The polyamine binding site in inward rectifier K^+ channels. J. Gen. Physiol. 2006; 127:467–480. [PubMed: 16606689]
35. Heginbotham L, MacKinnon R. The aromatic binding site for tetraethylammonium ion on potassium channels. Neuron. 1992; 8:483–491. [PubMed: 1550673]
36. Kavanaugh MP, et al. Multiple subunits of a voltage-dependent potassium channel contribute to the binding site for tetraethylammonium. Neuron. 1992; 8:493–497. [PubMed: 1550674]
37. Lenaeus MJ, Vamvouka M, Focia PJ, Gross A. Structural basis of TEA blockade in a model potassium channel. Nat. Struct. Mol. Biol. 2005; 12:454–459. [PubMed: 15852022]
38. Ahern CA, Eastwood AL, Lester HA, Dougherty DA, Horn R. A cation-pi interaction between extracellular TEA and an aromatic residue in potassium channels. J. Gen. Physiol. 2006; 128:649–657. [PubMed: 17130518]

39. Burley SK, Petsko GA. Amino-aromatic interactions in proteins. FEBS Lett. 1986; 203:139–143. [PubMed: 3089835]
40. Bremi T, Ernst M, Ernst RR. Side-chain motion with two degrees of freedom in peptides. An NMR study of phenylalanine side chains in antamanide. J. Phys. Chem. 1994; 98:9322–9334.
41. Hodgkin AL, Horowicz P. The influence of potassium and chloride ions on the membrane potential of single muscle fibres. J. Physiol. 1959; 148:127–160. [PubMed: 14402240]
42. Hagiwara S, Takahashi K. The anomalous rectification and cation selectivity of the membrane of a starfish egg cell. J. Membr. Biol. 1974; 18:61–80. [PubMed: 4854650]
43. Leech CA, Stanfield PR. Inward rectification in frog skeletal muscle fibres and its dependence on membrane potential and external potassium. J. Physiol. 1981; 319:295–309. [PubMed: 6976432]
44. Hagiwara S, Yoshii M. Effects of internal potassium and sodium on the anomalous rectification of the starfish egg as examined by internal perfusion. J. Physiol. 1979; 292:251–265. [PubMed: 573790]
45. Lu Z. Mechanism of rectification in inward-rectifier K^+ channels. Annu. Rev. Physiol. 2004; 66:103–129. [PubMed: 14977398]
46. Kubo Y, Baldwin TJ, Jan YN, Jan LY. Primary structure and functional expression of a mouse inward rectifier potassium channel. Nature. 1993; 362:127–133. [PubMed: 7680768]
47. Liman ER, Tytgat J, Hess P. Subunit stoichiometry of a mammalian K^+ channel determined by construction of multimeric cDNAs. Neuron. 1992; 9:861–871. [PubMed: 1419000]
48. Kubo Y, Reuveny E, Slesinger PA, Jan YN, Jan LY. Primary structure and functional expression of a rat G-protein-coupled muscarinic potassium channel. Nature. 1993; 364:802–806. [PubMed: 8355805]
49. Rascal N, et al. Expression of an atrial G-protein-activated potassium channel in Xenopus oocytes. Proc. Natl. Acad. Sci. U. S. A. 1993; 90:6596–6600. [PubMed: 8341673]
50. Guo D, Lu Z. Pore block versus intrinsic gating in the mechanism of inward rectification in strongly rectifying IRK1 channels. J. Gen. Physiol. 2000; 116:561–568. [PubMed: 11004205]
51. Guo D, Lu Z. IRK1 inward rectifier K^+ channels exhibit no intrinsic rectification. J. Gen. Physiol. 2002; 120:539–551. [PubMed: 12356855]
52. Huang CL, Feng S, Hilgemann DW. Direct activation of inward rectifier potassium channels by PIP2 and its stabilization by Gβγ. Nature. 1998; 391:803–806. [PubMed: 9486652]
53. Otwinowski Z, Minor W. Processing of X-ray diffraction data collected in oscillation mode. Methods Enzymol. 276:307–326. (21997).
54. Collaborative Computational Project, N.4. The CCP4 suite: programs for protein crystallography. Acta Crystallogr D Biol Crystallogr. 1994; 50:760–763. [PubMed: 15299374]
55. Navaza J. AMoRe: an automated package for molecular replacement. Acta Crystallographica. 2004; A50:157–163.
56. Jones TA, Zou JY, Cowan SW, Kjeldgaard M. Improved methods for building protein models in electron density maps and the location of errors in these models. Acta Crystallogr A. 1991; 47:110–119. [PubMed: 2025413]
57. Emsley P, Cowtan K. Coot: model-building tools for molecular graphics. Crystallographica Section D Biological Crystallography. 2004; 60:2126–2132.
58. Brunger AT, et al. Crystallography & NMR system: A new software suite for macromolecular structure determination. Acta Crystallogr. D. Biol. Crystallogr. 1998; 54:905–921. [PubMed: 9757107]
59. Laskowski RA, MacArthur MW, Moss D, Thornton JM. PROCKECH: a program to check the stereochemical quality of protein structures. Journal of Applied Crystallography. 1993; 26:283–291.
60. The PyMOL molecular graphics system on the world wide web. (http://www.pymol.org)

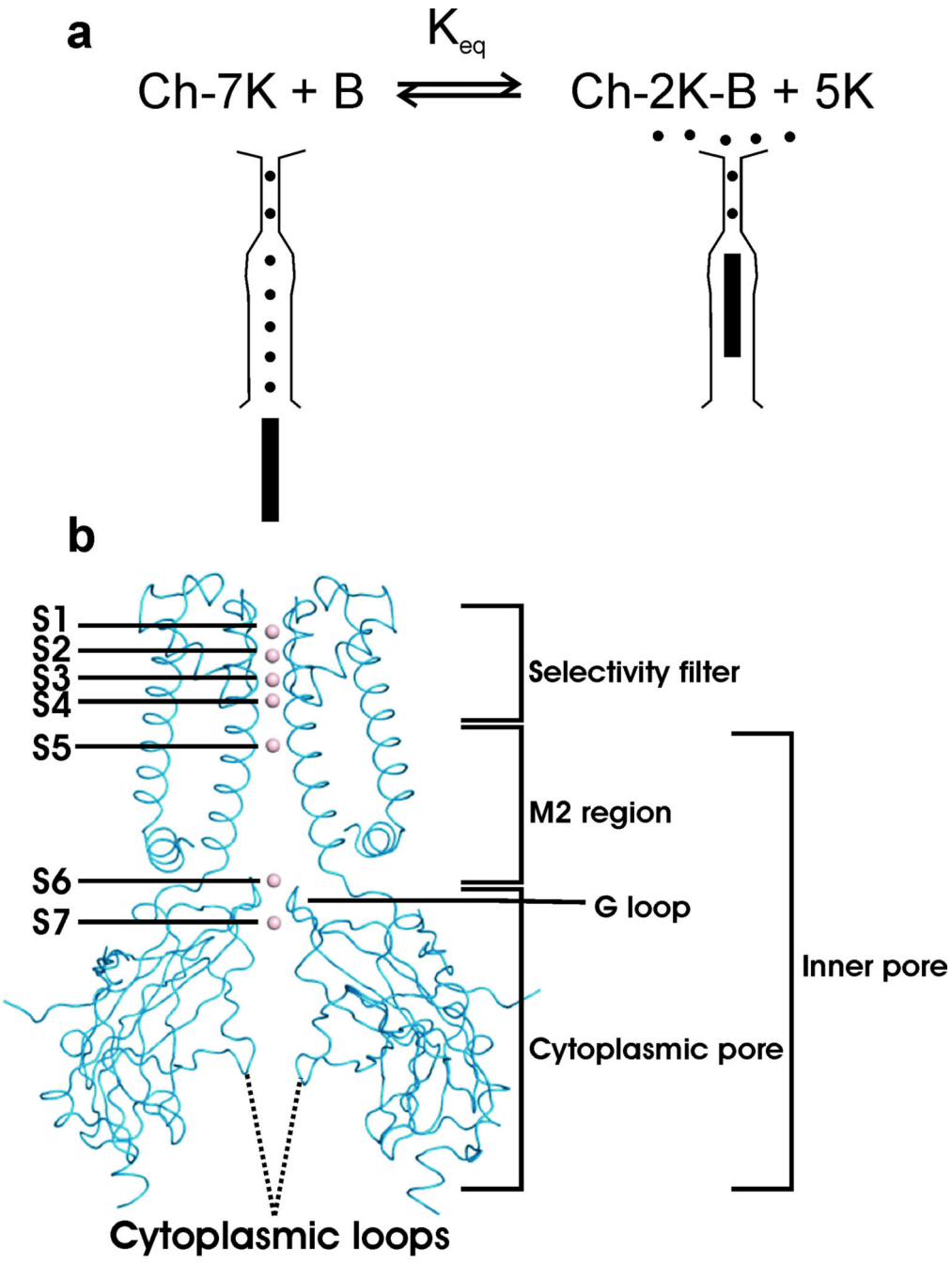

Figure 1.

Kinetic scheme and Kir structures. (a) Blocking reaction where the intracellular spermine blocker (denoted as "B") and five extracellular K^+ ions displace one another in a Kir channel (Ch). (b) Crystal structure of a Kir chimera (PDB 2QKS)[13] with seven ion sites. Two of four subunits are shown. The extracellular end is at top.

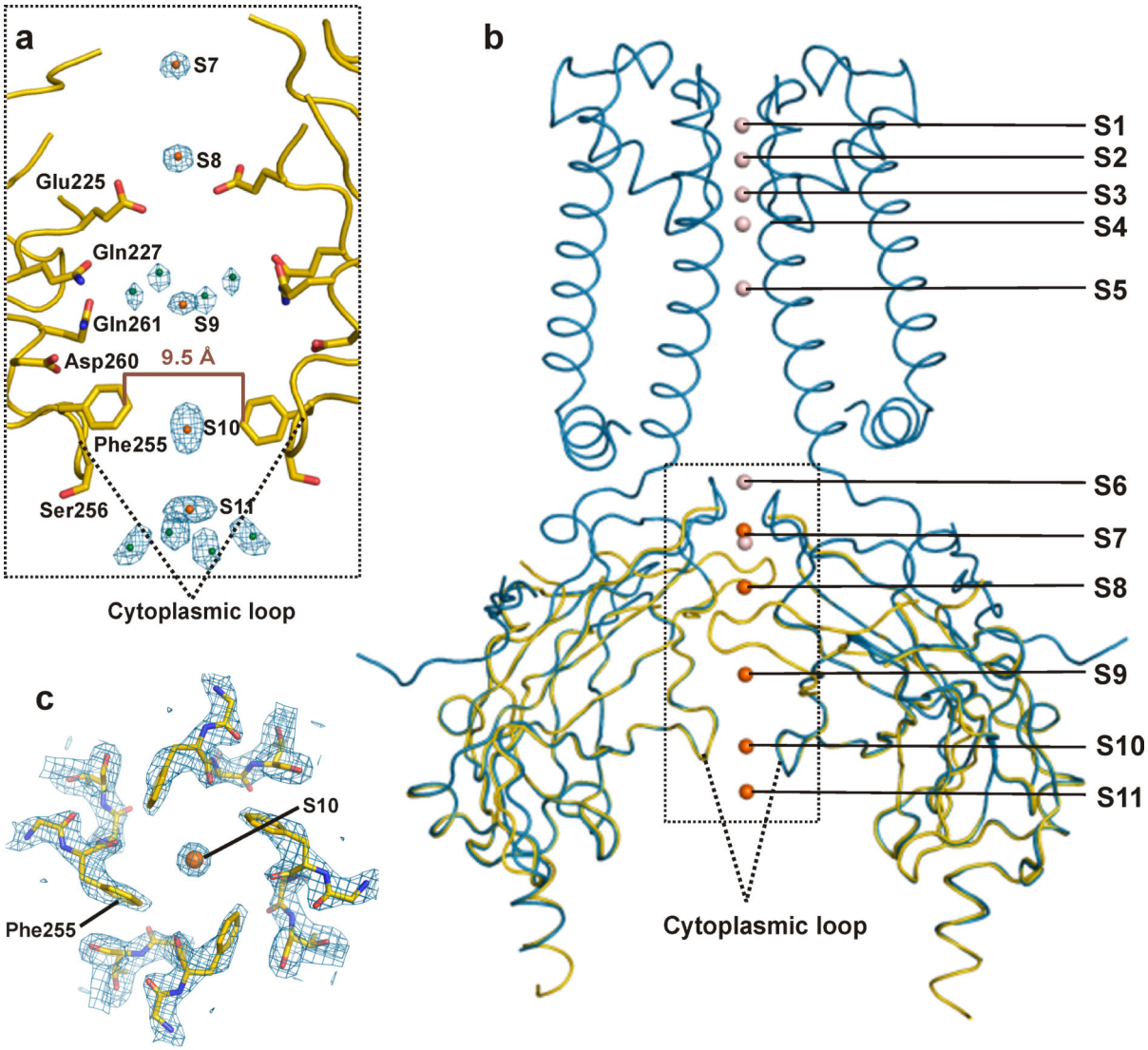

Figure 2.

Crystal structure model of the cytoplasmic pore. (a) Partial crystal structure model of the cytoplasmic pore of Kir3.1 containing the S225E mutation (approximately corresponding to the boxed region in panel b; two of four subunits are shown; intracellular end is at the bottom). The $2F_o - F_c$ composite-omit map contoured at 2.5 σ features densities (blue meshes) around the five ion sites, superimposed on the structure model. The map was calculated using a model that omits all ions and water molecules, as well as the side chain of six residues (sticks; Glu225, Gln227, Gln261, Asp260, Phe255 and Ser256) that interact directly or through water molecules with the newly identified ions at S8 – S11. Na^+ ions and water molecules are represented by orange and green spheres, respectively. Residues 41–43, 58–63, 190–192, 218–223, 303–306, 333–337 and 369 – 371, as well as the remaining part (Gly and Ser) of the N-terminal thrombin recognition sequence, are disordered. (b) Backbone structures of the cytoplasmic pore of S225E mutant Kir3.1 (yellow) and the Kir chimera[13] (blue; taken from Fig.1b) are superimposed. (c) Cross section of the $2F_o - F_c$

composite-omit map (2 σ) at the level of S10, showing the ion density and its immediate surroundings. The map was generated in the same way as for panel a.

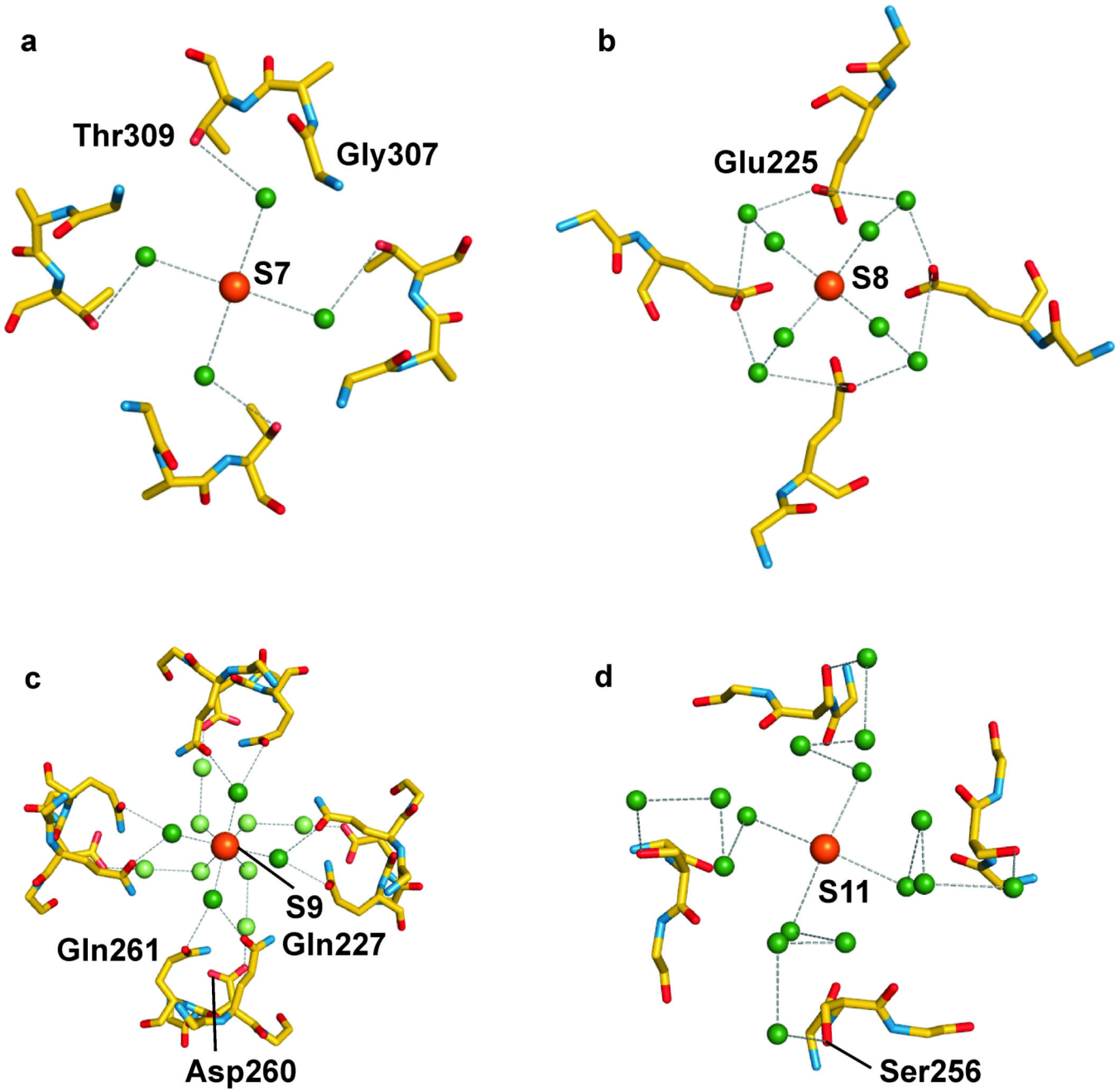

Figure 3.

Ions and surrounding water molecules. Local structures around S7 (a), S8 (b), S9 (c), and S11 (d). The ions and water molecules are shown as orange and green spheres, respectively. Dotted lines indicate presumed interactions.

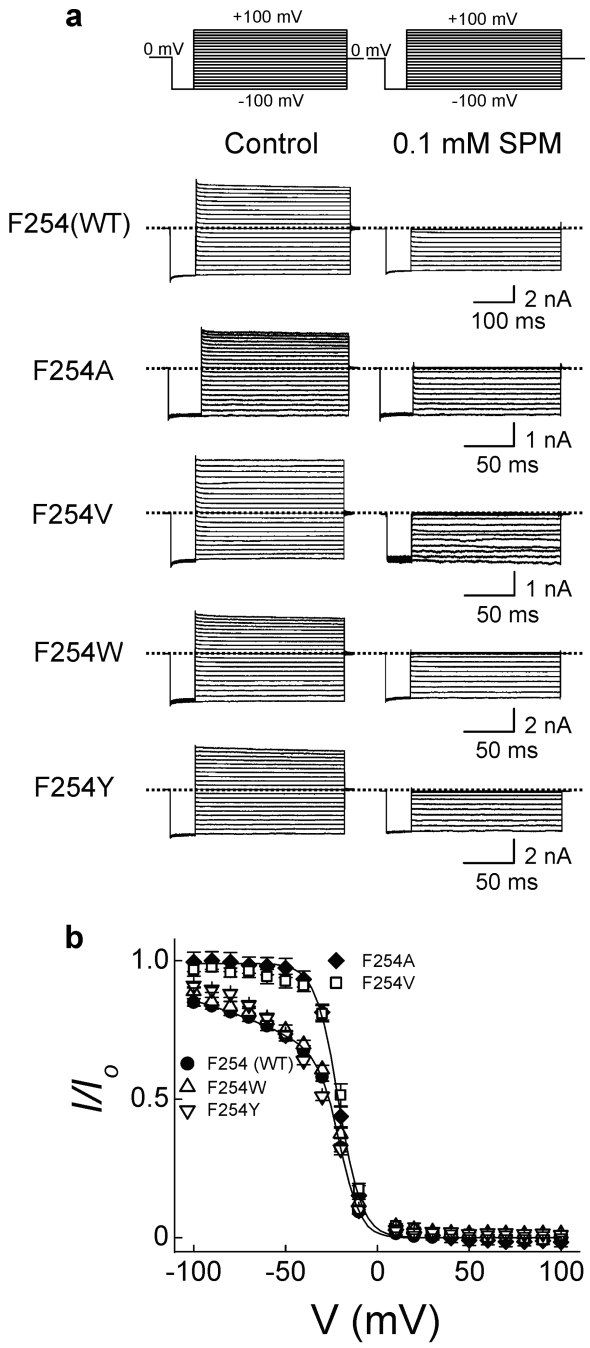

Figure 4.

Effects of mutations at Phe254 on spermine block of Kir2.1 channels. (a) Macroscopic currents of wild-type and mutant channels, recorded in the absence (control) and presence of 0.1 mM intracellular spermine with the protocols shown on top (a 3-fold lower spermine concentration was used for F254Y to offset its 3-fold higher affinity). The wild-type and F254A records are taken from Ref. 21. Dotted lines indicate zero current levels. (b) Fraction of currents (mean ± sem, n = 5–6) not blocked by spermine is plotted against membrane voltage for wild-type and mutant channels. The curve superimposed on the data from wild-

type, F254W, and F254Y channels is a previous fit (taken from Ref. 21) to the wild-type data, of a two-step sequential blocking model. Its parameters are: the dissociation constant for the first step K_1 (0 mV) = 1.30×10^{-4} M^{-1} with associated valence $Z_1 = 0.40$, and the "equilibrium" constant for the second step (K_2 at 0 mV) = 1.44×10^{-2} with associated valence $Z_2 = 4.2$. The curve superimposed on the data from F254A and F254V channels is a previous fit (taken from Ref. 21) to the F254A mutant data, of a single-step blocking model with parameters $K_d(0\ mV) = 3.82 \times 10^{-6}$ M^{-1} and $Z = 4.0$.

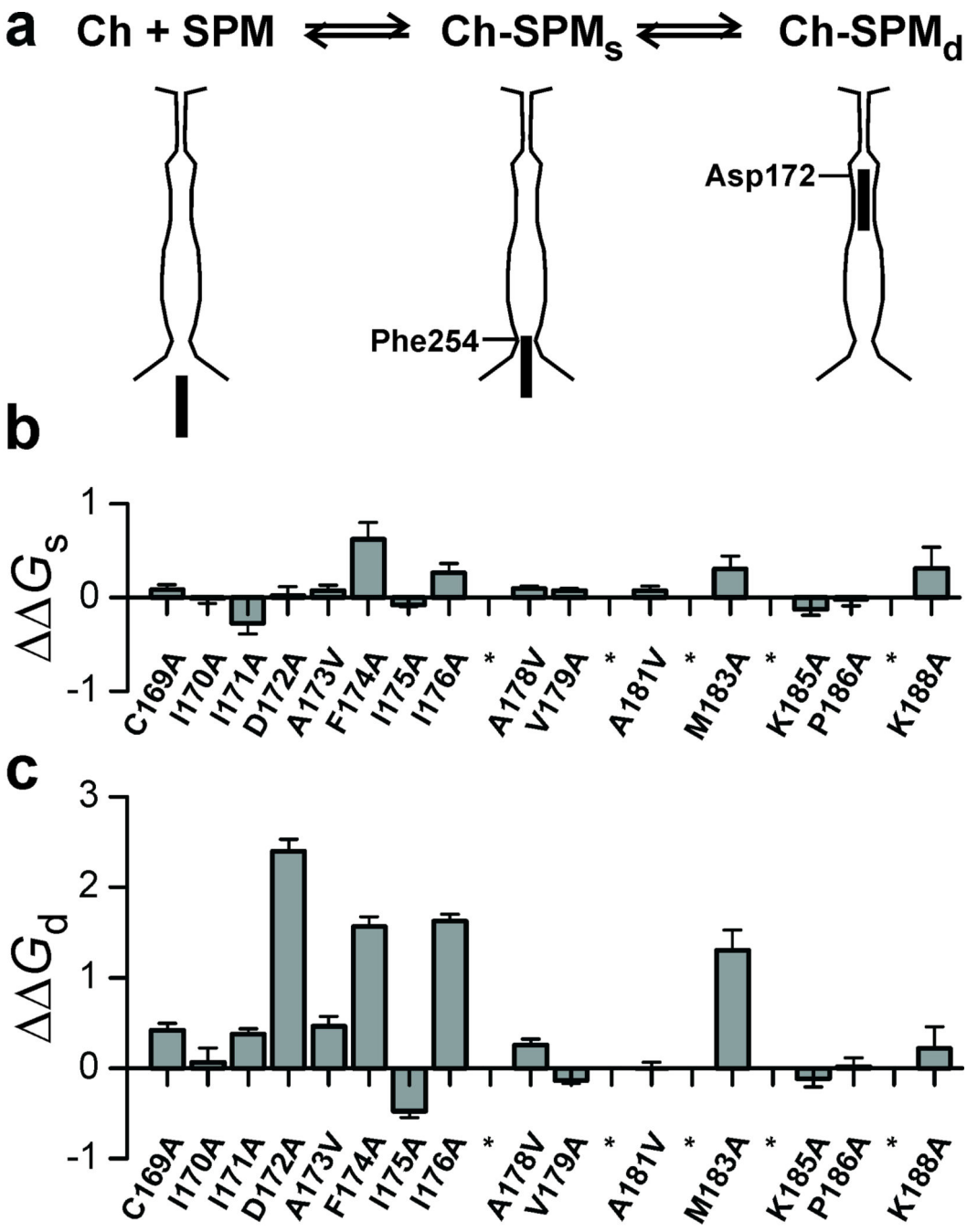

Figure 5.

Identification of mutations in M2 that affect spermine affinity of the deep site in Kir2.1. (a) Two-step spermine-blocking scheme for Kir2.1. (b, c) Free energy changes (mean ± sem, n = 5) of spermine interactions with the shallow (b) and deep (c) sites caused by the various mutations in M2. The energy changes were estimated from the “equilibrium” constants estimated as previously described[9, 21]. Asterisks indicate mutations that produced no measurable currents.

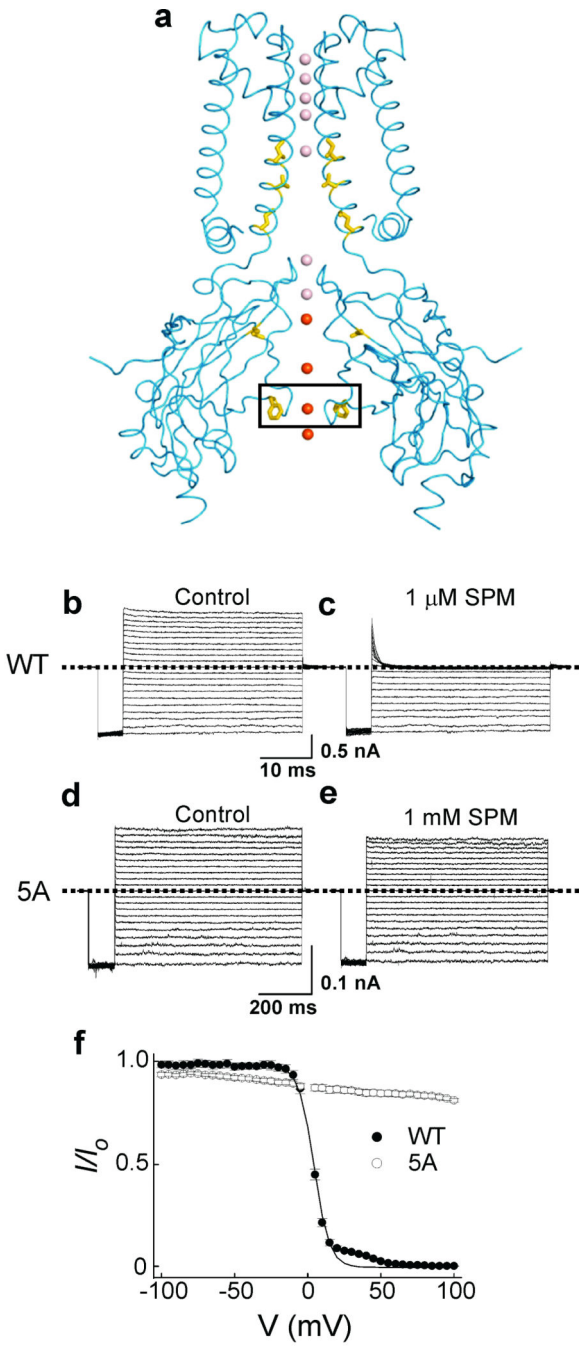

Figure 6.

A quintuple mutation abolishes spermine block of Kir2.1. (a) Structure of the chimera[13] in Fig. 1b, in which the five yellow colored residues (from top to bottom) correspond to Asp172, Ile176, Met183, Glu299 and Phe254 in Kir2.1. The box indicates the region of the cytoplasmic loop deleted in the ΔGFDS mutant shown in Fig. 7. (b–e) Currents of wild-type (b, c) and quintuple mutant (d, e) channels, recorded with the protocols shown in Fig. 4a and in the absence (b, d) or presence of 1 μM (c) or 1 mM (e) spermine (SPM). The quintuple mutant channel (5A) contains D172A, I176A, M183A, E299A and F254A mutations. Dotted

lines indicate zero current levels. (f) Fraction (mean ± sem, n = 5) of wild-type or 5A mutant currents not blocked by (1 μM or 1 mM) spermine, plotted against voltage.

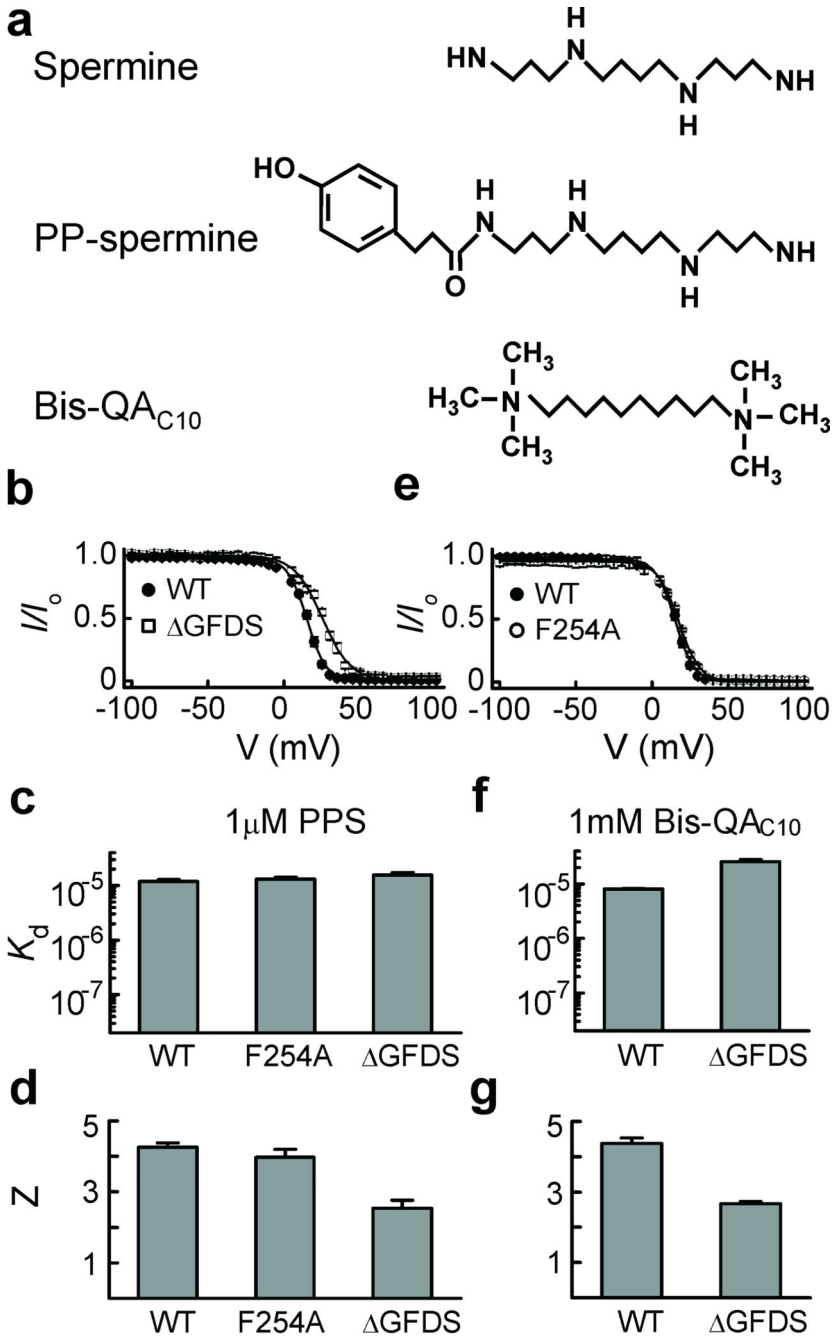

Figure 7.

Deleting the cytoplasmic loop lowers the valence of Kir2.1 block. (a) Chemical structures of spermine, PP-spermine and bis-QA_{C10}. (b–e) Fraction of wild-type channels and ΔGFDS (b) or F254A (e) mutant currents not blocked by 1 μM PP-spermine plotted against voltage. Curves through the data are fits of Boltzmann functions. K_d(0 mV) (c) and Valences Z (d) obtained from fits in panels b and e, summarized for PP-spermine blocking wild-type channels, and ΔGFDS or F254A mutant channels. (f, g) K_d(0 mV) (f) and valences Z (g) for

bis-QA_{C10} blocking wild-type and ΔGFDS mutant channels. All data in b–g are plotted as mean ± sem (n = 5).

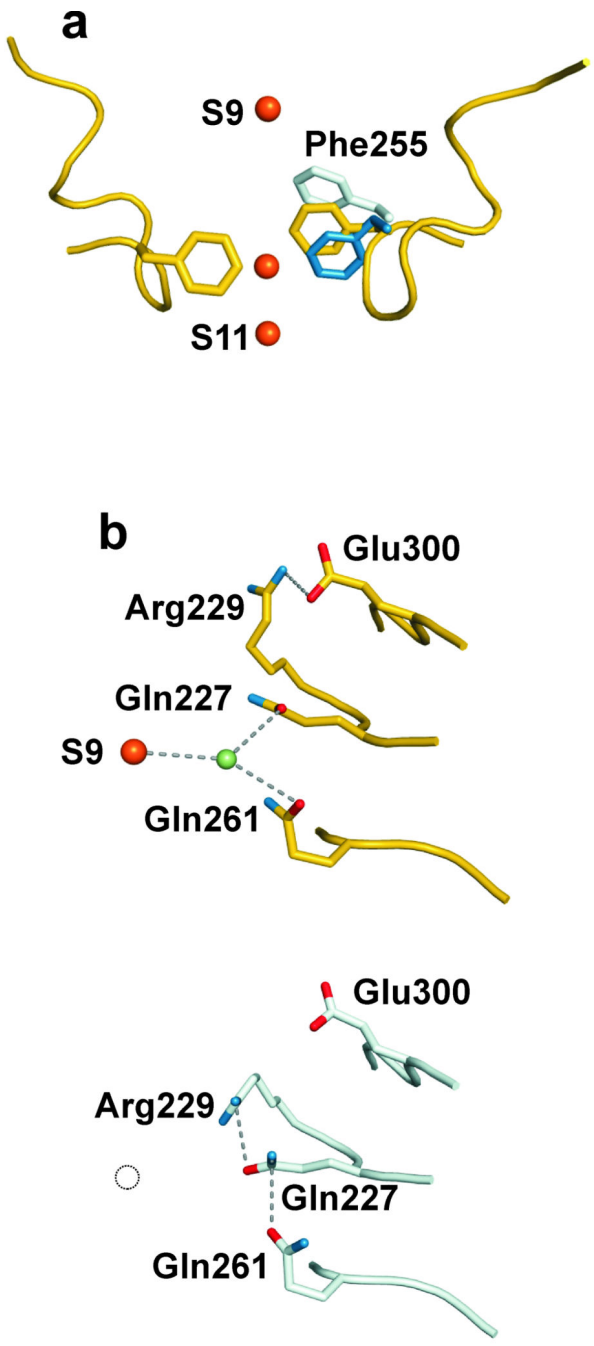

Figure 8.

Structural comparison of the isolated Kir3.1 cytoplasmic pore and the Kir chimera. (a) Local structure of Kir3.1's cytoplasmic pore around Phe255 (yellow). The side chains, colored blue and silver, are those of Phe255 in structural states A and B, respectively, of the Kir chimera[13]. Phe255 backbones of the three structures are superimposed. (b) R229 forms a hydrogen bond with a different neighboring residue in the structure of the isolated Kir3.1 cytoplasmic pore (upper) compared to that of the Kir chimera[13] (state B; lower). The ions and water molecules are shown as orange and green spheres (upper panel), respectively,

whereas the dotted circle indicates the expected S9 position. Presumed hydrogen bonds are indicated by dashed lines.

Table 1

Data collection and refinement statistics

	S225E mutant
Data collection	
Space group	$P42_12$
Cell dimensions	
a, *b*, *c* (Å)	77.46, 77.46, 86.72
Resolution (Å)	40 – 2.0 (2.07–2.00)*
R_{sym}	0.05 (0.35)
$I/\sigma I$	39.8 (7.7)
Completeness (%)	91.4 (100)
Redundancy	11.2 (10.5)
Refinement	
Resolution (Å)	40 – 2
No. reflections	16,749
R_{work} / R_{free}	25.4/26.6
No. atoms	
Protein	1386
Ligand/ion	5
Water	180
B-factors	
Protein	45.78
Ion	80.24
Water	59.40
R.m.s. deviations	
Bond lengths (Å)	0.0050
Bond angles (°)	1.220

A single crystal was used for both structure determination at 2.0 Å and refinement.

*Values in parentheses are for highest-resolution shell.